ICAS 2016
30th Congress of the International Council of the Aeronautical Sciences
DCC, Daejeon, Korea ; September 25-30, 2016

A DEVELOPMENT OF MESHLESS POINT GENERATION TECHNIQUE FOR ANALYSIS OF THE UNSTEADY FLOW AROUND THE MULTI-BODY

Jae Sang Rhee*, Jin Young Huh*, Dabin Han*, Kyu Hong Kim, Suk Young Jung*****
Department of Mechanical & Aerospace Engineering, Seoul National University,
****Department of Mechanical Engineering/Institute of Advanced Aerospace Technology, Seoul National University,***
*****Agency for Defense Development***

Keywords:*Meshless Algorithm, Gridless Algorithm, Moving Boundaries, Point Generation Technique*

Abstract

A meshless scheme is considered to be a useful method for analysis of the flow around difficult geometry in Computational Fluid Dynamics (CFD) field. For example, moving boundaries or highly-complex body. In order to analyze such a complicated flow, a meshless point generation technique for the unsteady flow around the multiple body including movement is developed in this study. Then, using the developed meshless point system, numerical analysis of unsteady flow considering the multi-body are carried out.

1 Introduction

Generally known finite volume method (FVM) in Computational Fluid Dynamics (CFD) requires mesh as a computational domain. In recent years, practical engineering application has been required in the field, along with the achievement of high performance of computing power. However, when using mesh-based method, it is known to be hard to handle the mesh for complex geometries. Moreover, considering a moving boundary, the problem become more crucial. It has been regarded as a conundrum for the researcher studying CFD. In order to alleviate the burden of generation computational domain, many kinds of methods have been suggested. For this reason, A meshless method has been studied some researchers [1]. As the name indicates, meshless methods only requires clouds of points. As mentioned before, research about meshless methods aim to develop the technique which is available to highly-complicated geometries, Such as separation motion of shroud. For the sake of development of meshless methods considering moving boundaries, some researchers have studied for meshless method for unsteady flow including movement [2], [3]. However, previous research have not considered all kind of moving, such as 6-DOF motion or large displacement. Consequently, point generation technique which considers a wide variety of moving problem is developed in this study. In order to treat the moving points efficiently; two point systems are suggested. The prismatic point system and the background point system. The prismatic point system is generated along the wall boundary. Its concept is same as in the prism layer in the unstructured grid [5]. This point system is used for efficient treatment for the moving point system. And the background point system is generated using Cartesian grid point. Using two different point system, computational domain for the unsteady flow considering multi-body is generated. For validation of the developed technique, an analysis of the flow around pitching NACA0012 airfoil is carried out and the results are compared with the AGARD [6] CT 5 test case. Then, in order to verify the applicability of the multiple boundaries, the simulation of the flow around a multi-element airfoil with flap deflection is also carried out. The Williams airfoil (Configuration B) [7] is selected as validation case. And the results are compared with the result of the grid deformation method

[10]. Least Squares Method with AUSMPW+[4], [8] is used as a spatial discretization method, and LU-SGS [9] is selected as a time integration scheme. As a limiting process, Minmod limiter is used.

2 Flow solution

2.1 Least Squares Method

Consider Taylor series expansion with the ignorance of high order terms, as shown in Eq. (1). In the Meshless method, In order to find the unknown derivative terms of Eq. (1), Least Squares Method has been used.

$$\varphi(x,y) = \varphi_0 + \Delta x\frac{\partial\varphi(x_0)}{\partial x} + \Delta y\frac{\partial\varphi(y_0)}{\partial y} + O(\Delta^2) \quad (1)$$

The Least Squares Method with weighted function can be expressed as

$$\min\sum_{j=1}^{n}\omega_{0j}\left[\Delta\varphi_{0j} - \Delta x_{0j}\frac{\partial\varphi(x_0)}{\partial x} - \Delta y_{0j}\frac{\partial\varphi(y_0)}{\partial y}\right]^2 \quad (2)$$

$$\frac{\partial\varphi}{\partial x} \approx \sum_j a_{0j}(\varphi_j - \varphi_0) \quad (3)$$

$$\frac{\partial\varphi}{\partial y} \approx \sum_j b_{0j}(\varphi_j - \varphi_0) \quad (4)$$

where, n indicates the number of point in the vicinity which is called local point cloud. For a two-dimensional space, the calculated coefficients are as follows.

$$a_{0j} = \frac{\omega_{0j}\Delta x_{0j}\sum(\omega\Delta y^2) - \omega_{0j}\Delta y_{0j}\sum(\omega\Delta x\Delta y)}{\sum(\omega\Delta x^2)\sum(\omega\Delta y^2) - (\sum\omega\Delta x\Delta y)^2} \quad (5)$$

$$b_{0j} = \frac{\omega_{0j}\Delta y_{0j}\sum(\omega\Delta x^2) - \omega_{0j}\Delta x_{0j}\sum(\omega\Delta x\Delta y)}{\sum(\omega\Delta x^2)\sum(\omega\Delta y^2) - (\sum\omega\Delta x\Delta y)^2} \quad (6)$$

A simple inverse distance weighting function [14] is used to improve accuracy

$$\omega_{0j} = \frac{1}{\left(\Delta x_{0j}^2 + \Delta y_{0j}^2\right)^{1/2}} \quad (7)$$

2.2 Governing equations and numerical schemes

In this study, the two-dimensional Euler equation is selected as governing equations. Euler equations in Arbitrary Largrangian Eulerian (ALE) form is written as

$$\frac{\partial\omega}{\partial t} + \frac{\partial f}{\partial x} + \frac{\partial g}{\partial y} = 0 \quad (8)$$

$$\omega = \begin{bmatrix}\rho\\ \rho u\\ \rho v\\ \rho E\end{bmatrix}, f = \begin{bmatrix}\rho U\\ \rho uU + p\\ \rho vU\\ \rho EU + pu\end{bmatrix}, g = \begin{bmatrix}\rho V\\ \rho uV\\ \rho vV + p\\ \rho EV + pv\end{bmatrix} \quad (9)$$

$$E = \frac{p}{(\gamma-1)\rho} + \frac{1}{2}(u^2+v^2), H = E + \frac{p}{\rho} \quad (10)$$

In Eq. (9), U and V denote the contravariant velocities, and it is defined as follows

$$U = (u - u_p), V = (v - v_p)$$

where, u_p and v_p are the components of the velocity of a point in the x, y direction respectively.

Then, Eq. (8) can be expressed as follows

$$\frac{\partial\omega_i}{\partial t} + \sum_{j=1}^{n} a_{ij}\Delta f_{ij} + \sum_{j=1}^{n} b_{ij}\Delta g_{ij} = \frac{\partial\omega_i}{\partial t} + \sum_{j}^{n}\Delta F_{ij} = 0 \quad (11)$$

where, $F = af + bg$ is a directed flux along the metric weight vector (a,b). To improve accuracy and robustness, AUSMPW+ is modified for the Meshless method for the spatial discretization. This scheme use midpoint flux at $j + 1/2$ instead of the flux at j, as shown in Eq. (12)

$$\sum_{j=1}^{n}\Delta F_{ij} = 2\sum_{j=1}^{n}\Delta F_{ij+\frac{1}{2}} = 2\sum_{j=1}^{n}\left(F_{ij+\frac{1}{2}} - F_{ij}\right) \quad (12)$$

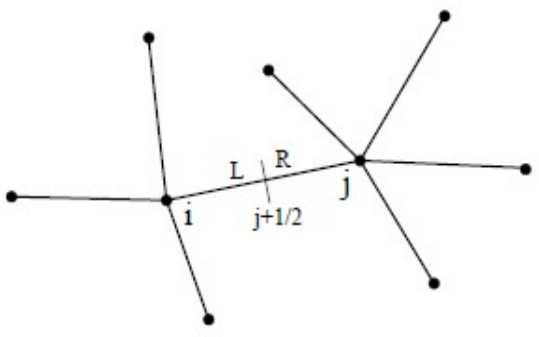

Figure 1 illustration of mid-point value on the edge connecting nodes i and j

$F_{ij+1/2}$ can be obtained from AUSMPW+ scheme. The numerical flux of AUSMPW+ is given as follows.

$$F_{\frac{1}{2}} = \bar{M}_L^+ c_{\frac{1}{2}}\Phi_L + \bar{M}_R^- c_{\frac{1}{2}}\Phi_R + (P_L^+ P_L + P_R^- R_R) \quad (13)$$

where, $\Phi = (\rho, \rho u, \rho H)$ and $P = (0, p, 0)^T$. The subscripts '1/2', 'L' and 'R' mean a quantity at a midpoint on the edge in Figure 1 and at the left and right states across the edge, repectively. The mach number at the midpoint is defined as

$$m_{1/2} = M_L^+ + M_R^- \tag{14}$$

$\bar{M}_L^+$ and $\bar{M}_R^-$ can then be computed by
If $m_{1/2} \geq 0$, then,

$$\bar{M}_L^+ = M_L^+ + M_R^-[(1-w)(1+f_R) - f_L] \tag{15}$$

$$\bar{M}_L^- = M_R^- w(1+f_R) \tag{16}$$

Else if $m_{1/2} < 0$, then,

$$\bar{M}_L^+ = M_L^+ + w(1+f_L) \tag{17}$$

$$\bar{M}_R^+ = M_R^- + M_L^+[(1-w)(1+f_L) - f_R] \tag{18}$$

where,

$$w(P_L, P_R) = 1 - \min\left(\frac{P_L}{P_R}, \frac{P_R}{R_L}\right)^3 \tag{19}$$

The pressure-based weight function is simplified to

$$f_{L,R} = \left(\frac{P_{L,R}}{P_s} - 1\right) * \min\left(1, \frac{\min(LCP_{i,j})}{\min(P_L, P_R)}\right)^2, P_s \neq 0 \tag{20}$$

where,

$$P_s = P_L^+ P_L + P_R^- P_R \tag{21}$$

The split Mach number is defined by

$$M^{\pm} = \begin{cases} \pm\frac{1}{4}(M \pm 1)^2, & |M| \leq 1 \\ \frac{1}{2}(M \pm |M|), & |M| > 1 \end{cases} \tag{22}$$

$$P^{\pm} = \begin{cases} \pm\frac{1}{4}(M \pm 1)^2(2 \mp M), & |M| \leq 1 \\ \frac{1}{2}(1 \pm sign(M)), & |M| > 1 \end{cases} \tag{23}$$

The Mach number of each side is

$$M_{L,R} = \frac{U_{L,R}}{c_{1/2}} \tag{24}$$

And the speed of sound $(c_{1/2})$ is

$$c_{1/2} = \begin{cases} \min\left(\frac{c^{*2}}{max(|U_L|, c^*)}\right), & \frac{1}{2}(U_L + U_R) > 0 \\ \min\left(\frac{c^{*2}}{max(|U_R|, c^*)}\right), & \frac{1}{2}(U_L + U_R) < 0 \end{cases} \tag{25}$$

where,

$$c^* = \sqrt{2(\gamma-1)/(\gamma+1)H_{normal}} \tag{26}$$

$$H_{normal} = \frac{1}{2}\left(H_L - \frac{1}{2}V_L^2 + H_R - \frac{1}{2}V_R^2\right) \tag{27}$$

For a time integration, LU-SGS method, considering Dual time stepping, modified for meshless method is used [4]. More detailed explanation of the method can be found in [11].

3 Point generation methodology considering the movement of wall boundaries

3.1 HYCAPS method

In this study, we introduced 'Hybrid of Cartesian And Prismatic Point System' (HYCAPPS) method. As the name indicates, this method combines two point systems. The first point system is Prismatic Point System (PPS), and the other is Background Point System (BPS). PPS is created to consider boundary layer in the viscous flow. It is generated along the wall surface. The concept is same as the prismatic grid of FVM. It is shown in Figure 2

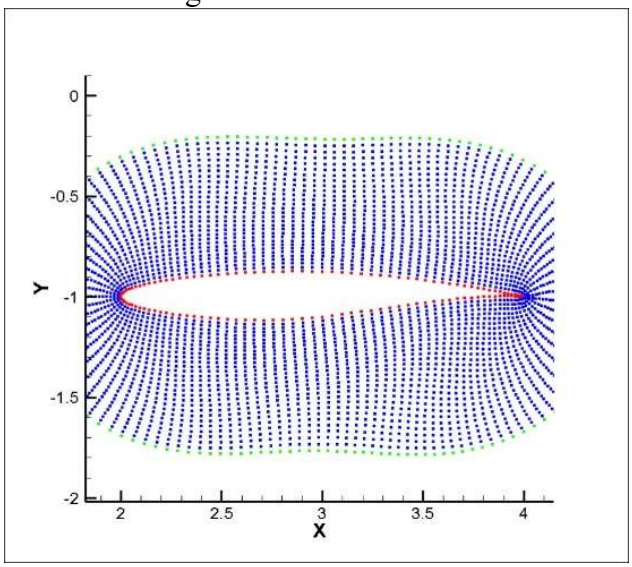

Figure 2 : the prismatic point system of RAE2822

Then, BPS can be obtained from Cartesian grid as shown in Figure 3. A detailed description of this method can be found in [12]. At the initial stage, the point systems may overlap each other. Because we generate the point systems independently. However, the overlap points must

be excluded when computing the flow solution. Therefore, we give the priority to each point system. A detailed description is as follows.

- The prismatic point systems always have priority compared to the background systems
- If the prismatic point systems overlap each other, the point which belongs to the lower level of layer has a higher priority. the concept of the level of layer is denoted in (a) of Figure 5. If the level is the same, the lower object number has a higher priority. Example is shown in (b) of Figure 5. The overlap points are shown with their indices. To explain in more detail, the point '1' belongs to the 'n+1' level layer of object '2' but this point is inside the 'n' level layer of object '1'. According to these rules, 1, 2, 7, 9 points are excluded from computational domain. But these points are not erased but switched off temporarily. Because we may use and consider these points again, in case of the reconstruction of computational domain according to movement of the object.
- If the background point systems overlap each other, the point system, which has the lower space of the grid, has a higher priority

Consequently, an example of the meshless point system generated by the aforementioned rules is shown in Figure 6. In the generated point system. local point cloud must be composed for all the computational point. It is also described in [12]

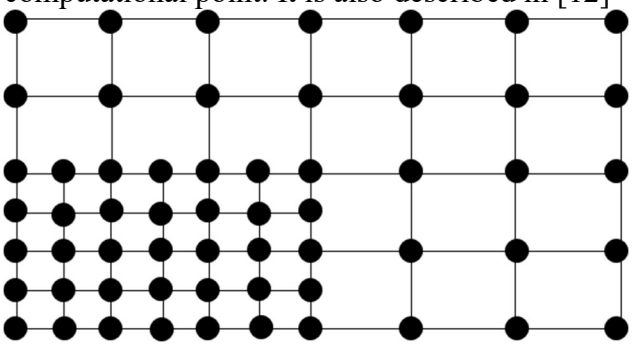

Figure 3 Cartesian grid points

HYCAPPS method makes it easy to handle points when the wall boundaries are moving, because it is easy to find an index of Cartesian grid point when the coordinates of a prismatic point is given.

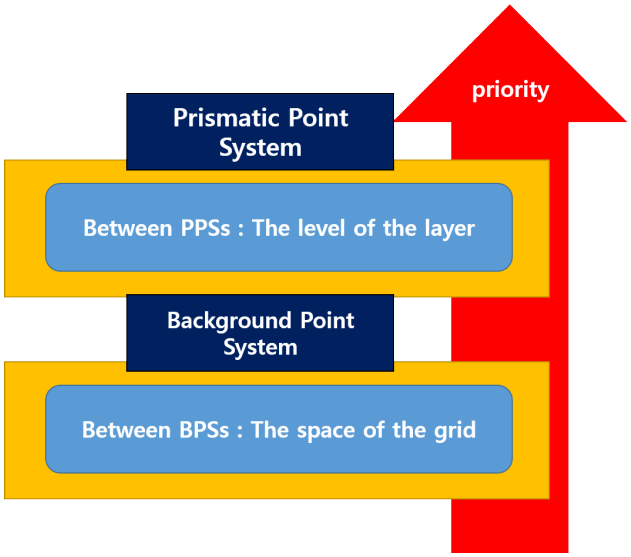

Figure 4 the rules of priority

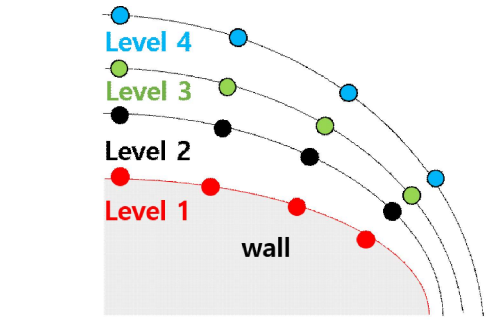

(a) The level of layer

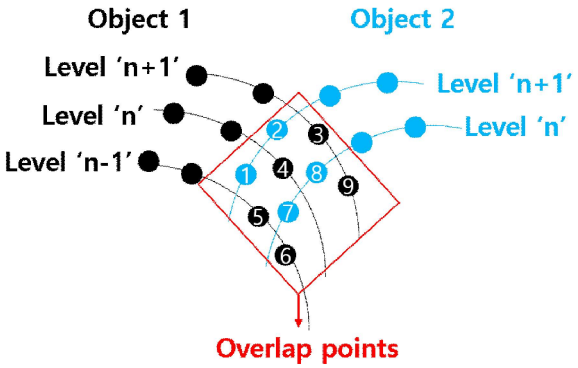

(b) Overlap points

Figure 5 the detailed explanation of the level of layer

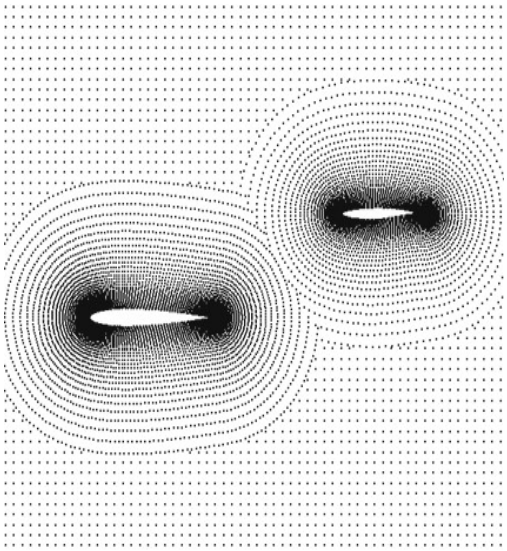

Figure 6 the complete meshless point system

3.2 Strategy for the moving boundaries

When the wall boundaries move, the meshless point system must be reconstructed. The process of the reconstruction is denoted in Figure 7.

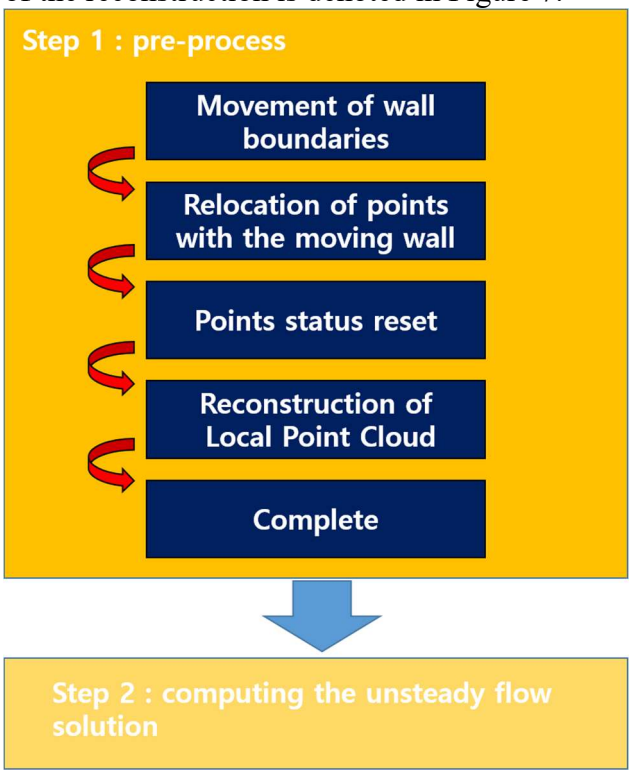

Figure 7 the process of the reconstruction

Relocation of points is carried out as follows

.

- The prismatic point systems move with the same linear and angular velocities of their objects, on the contrary, the background point systems remain static as shown in Figure 8
- Determine which points are to be 'off' or 'on' by the rule
- Reset the point distribution from the determination as shown in Figure 10

After the reset of the point distribution, local point cloud must be regenerated for the computational points. However it is highly time-consuming work, if we regenerate the local point cloud for all the computational point. In order to enhance the time efficiency, we introduce a condition which is called 'Vicinity Existence Test' (VEXT). In this study, we use 8 points in VEXT condition for both prismatic point and background point. Regardless of the type of the point system, there must be 8 points around a point except boundary point as shown in Figure 11. If all 8 vicinity points are 'on' state, that point use previous local point cloud. Using this method, only the points which don't satisfy 'VEXT' condition must generate new local point cloud. From this process, the time generating local point cloud for the computational domain for the next physical time can be saved.

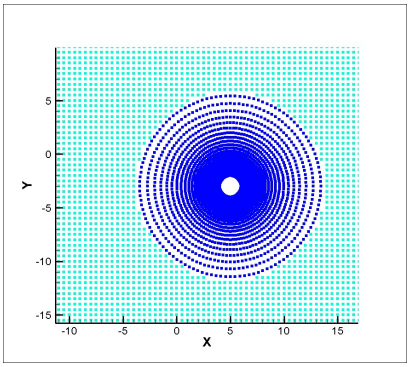

Figure 8 initial state

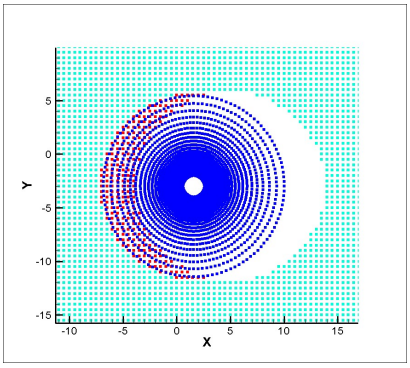

Figure 9 overlap arise from the movement

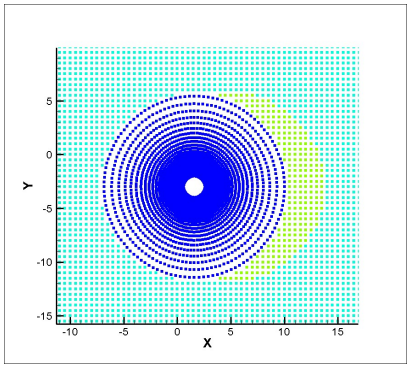

Figure 10 reset point distribution

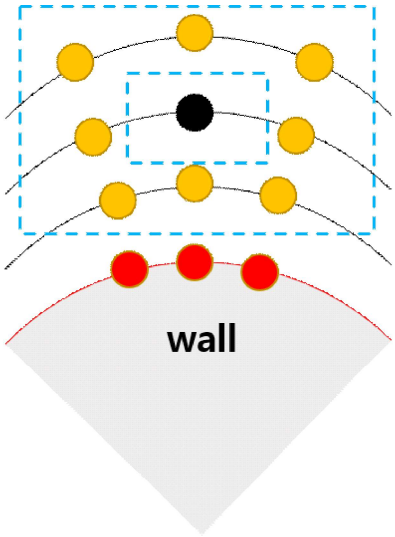

(a) 8 vicinity points of prismatic point

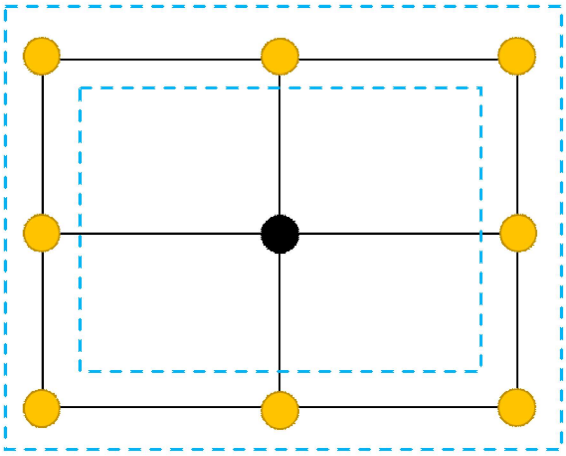

(b) 8 vicinity points of background point

Figure 11 'VEXT' condition

4 Results

4.1 Unsteady flow around the cylinder

The first validation case is the supersonic flow around the cylinder. We carried out computation for four cases. Every case has different freestream Mach number but the Mach numbers observed in the cylinder are equal to 2 and angle of attacks are equal to 0. The point systems are all same for all the case as shown in Figure 12. More information are written in Table 1 and Figure 12. This validation model was selected to show that results for four cases are same. We select the steady state result (case 4) as a reference. Figure 13 shows the pressure coefficient line along the surface and the stagnation line. It shows that we can obtain quite same result for all cases. Even though the computational domains are different each physical time step.

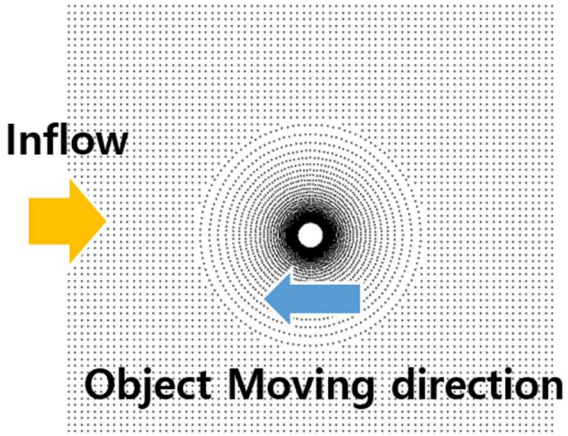

Figure 12 computational domain and the direction of freestream and the cylinder

Table 1 information for the flow condition

Case	Freestream Mach number	Mach number of the cylinder
1	0.0	2.0
2	1.0	1.0
3	1.5	0.5
4(reference)	2.0	0.0

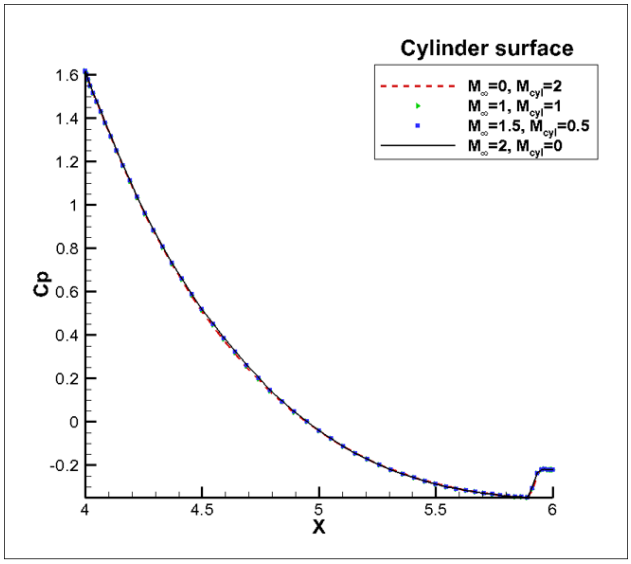

(a) Cylinder Surface

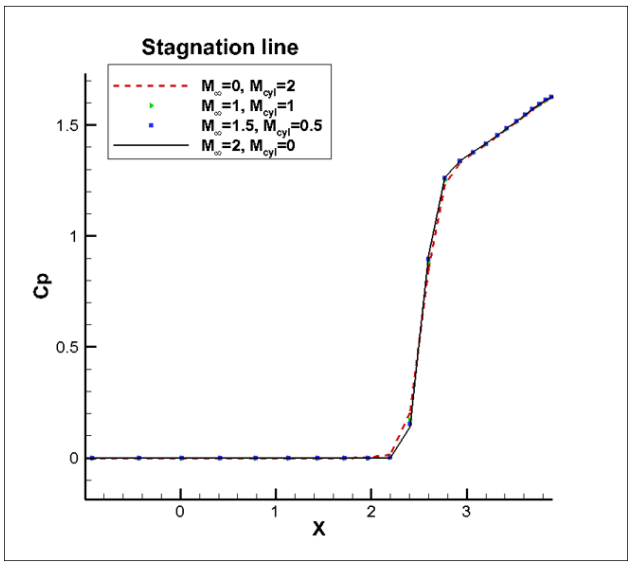

(b) Stagnation Line

Figure 13 pressure coefficient distribution of the moving cylinder

4.2 Unsteady flow around the oscillating NACA0012 airfoil

The next validation model is the unsteady flow around the oscillating NACA0012 airfoil. The results are compared with the AGARD experimental data [6] and Kirshmen's result from the Cartesian Grid Method [13]. The airfoil oscillates about its quarter chord. The oscillating motion of the airfoil is expressed as

$$\alpha = \alpha_0 + \alpha_m \sin(\omega t) \tag{28}$$

where α_0 is the mean incidence, α_m is the amplitude of the pitching oscillation, ω is the angular frequency of the oscillation. And instead of using ω, reduced frequency k is used for the computation. Reduced frequency is given as follows.

$$k = \frac{\omega c}{2V_\infty} \tag{29}$$

here, c is the chord length of the airfoil and V_∞ is the freestream speed. The conditions are as follows

$$\begin{cases} M_\infty = 0.755 \\ \alpha_0 = 0.016^o \\ \alpha_m = 2.51^o \\ k = 0.0814 \end{cases}$$

Before the unsteady computation, a calculation for the steady state flow is carried out. The computational domain and the steady state result are shown in Figure 14 and 15 respectively.
The physical time step is 1/64 of the period. And we compared lift coefficient and the pressure coefficient along the surface with the reference data. The results are shown in Figure 16~19.

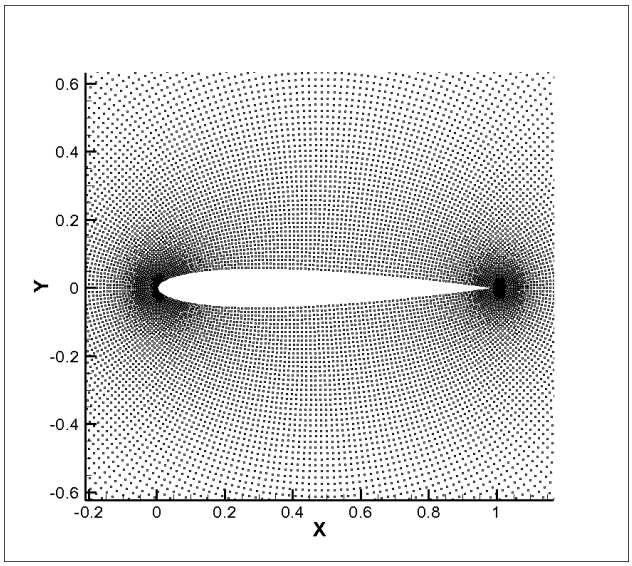

Figure 14 meshless point system for NACA0012

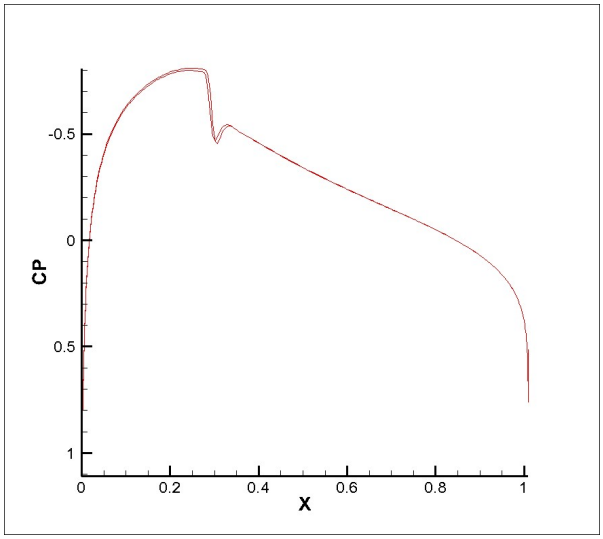

Figure 15 pressure coefficient of NACA0012 at steady state (mean incidence angle)

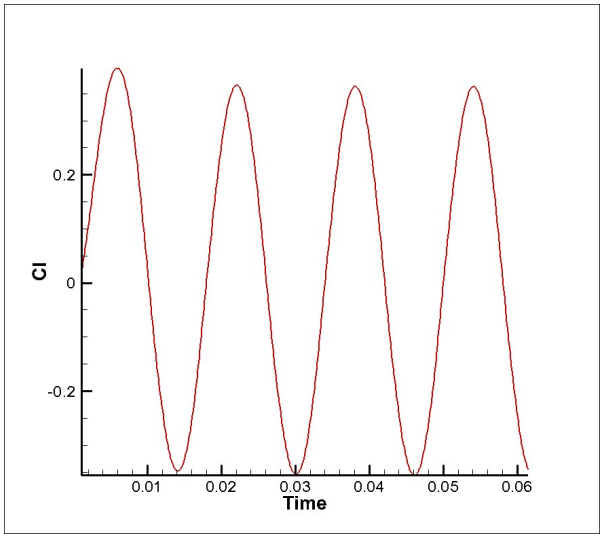

Figure 16 lift coefficient variation in time

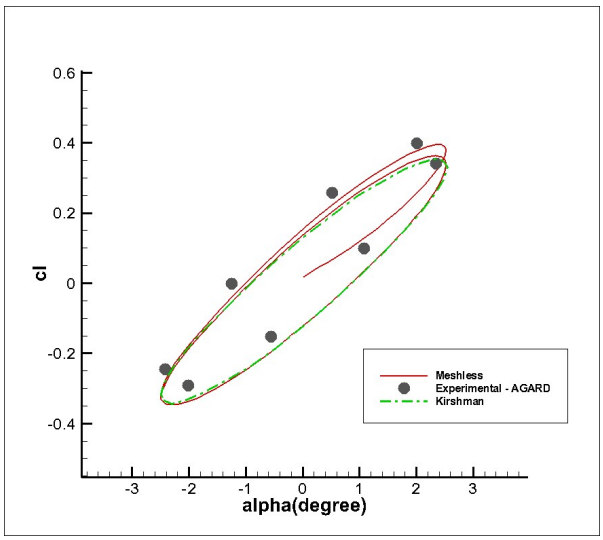

Figure 17 lift coefficient variation in pitching angle

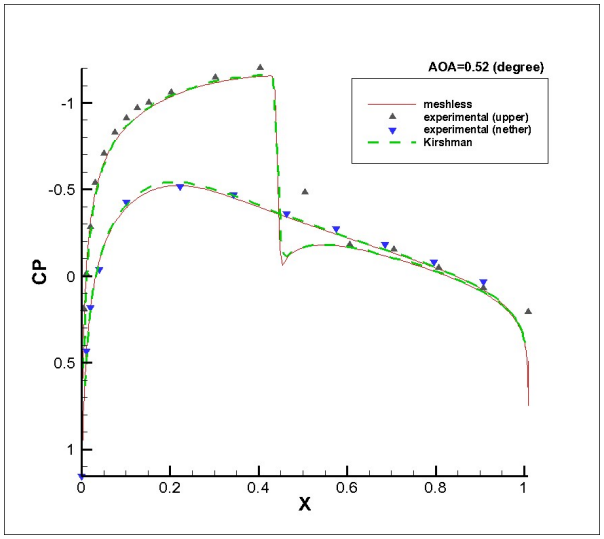

Figure 18 pressure coefficient distribution along the surface ($\alpha = 0.52^{o}$, phase angle $= 168^{o}$)

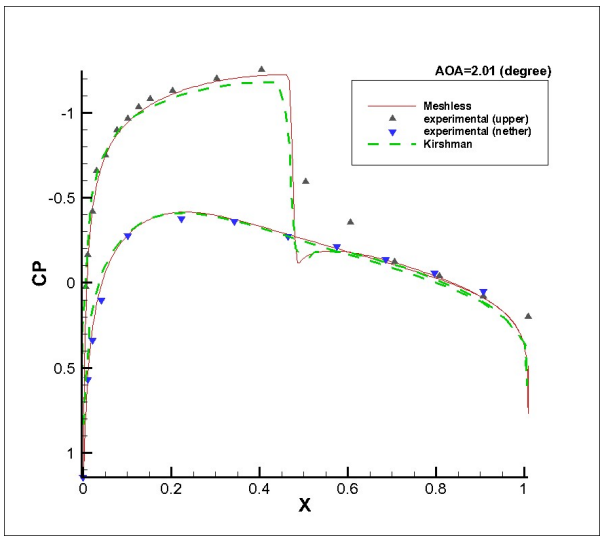

Figure 19 pressure coefficient distribution along the surface ($\alpha = 2.01^{o}$, phase angle $= 127^{o}$)

The results indicate that the developed point generation technique and the meshless method are robust and accurate compared to the conventional method.

4.2 Unsteady flow around the oscillating NACA0012 airfoil

For the demonstration of the performance of the point generation method, Williams airfoil (Configuration B) [7] with an oscillating flap is considered. In the case, Main airfoil is static, but the flap deflect from 0^{o} to 14^{o}. There are two prismatic point systems (Main airfoil and flap) and a variety of background point systems. The meshless point systems are shown in Figure 20

and 21 for the flap deflection angle 0º and 14º. If the flap deflects, the prismatic point system of the flap moves with the same velocity. On the contrary, the other point systems are stationary. It indicates that the methodology allows large and general movement. The flow solution is computed at atmospheric condition with freestream Mach number 0.58. 20,000 points are used for computational domain at the deflection angle 0º. However, the number of points is different from the deflection angle. Then, the deflection angle is given as follows.

$$\alpha = \alpha_0 + \alpha_m \sin(\omega t) \qquad (30)$$

where, α_0 is the mean incidence angle, α_m is the amplitude of the oscillation, and the reduced frequency is given as $k = \omega c / 2V_\infty$. And these values are as follows.

$$\begin{cases} \alpha_0 = 7.0^o \\ \alpha_m = 7.0^o \\ k = 0.0814 \end{cases}$$

The flap oscillates about the point located in front of its leading edge. We obtained steady state solution at the deflection angle 0º. Then, we regard reference length as chord length of the main airfoil. Pressure contours and the normal force coefficient are presented. And the normal coefficient result is compared with the result obtained from L. Dubac's grid deformation technique [10].

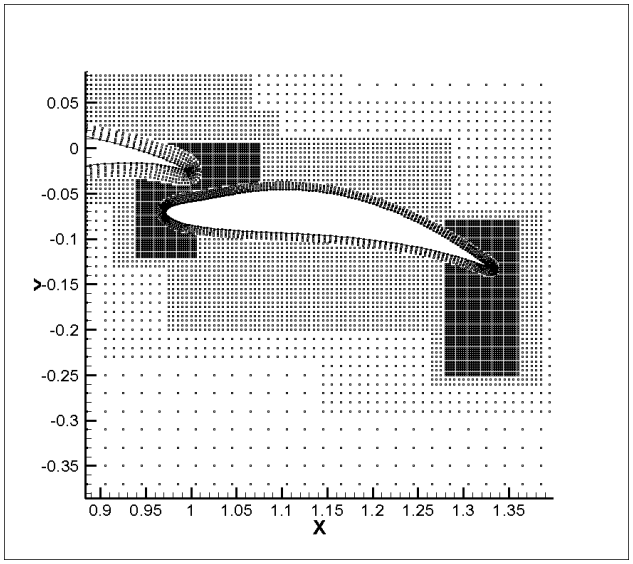

Figure 20 computational point at deflection angle 0º

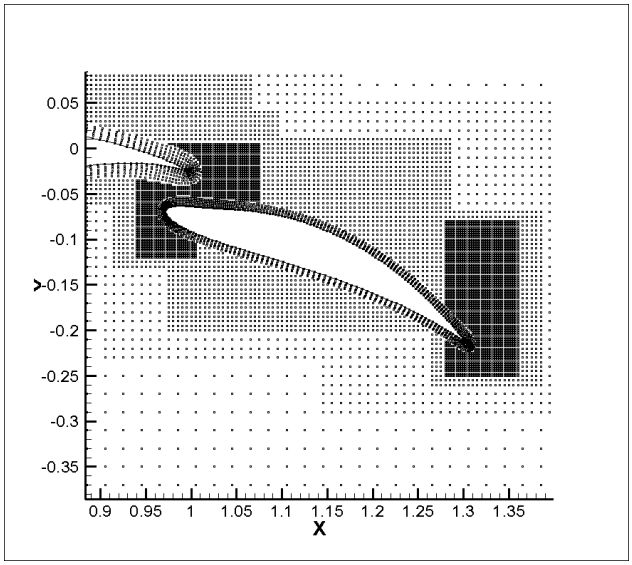

Figure 21 computational point at deflection angle 14º

The results are denoted in Figure 22~26. Figure 22 shows the lift coefficient comparison with result obtained by the grid deformation method. a slight difference can be seen from the result. Its maximum error is about 1.1%. This error may be attributed to the grid difference.

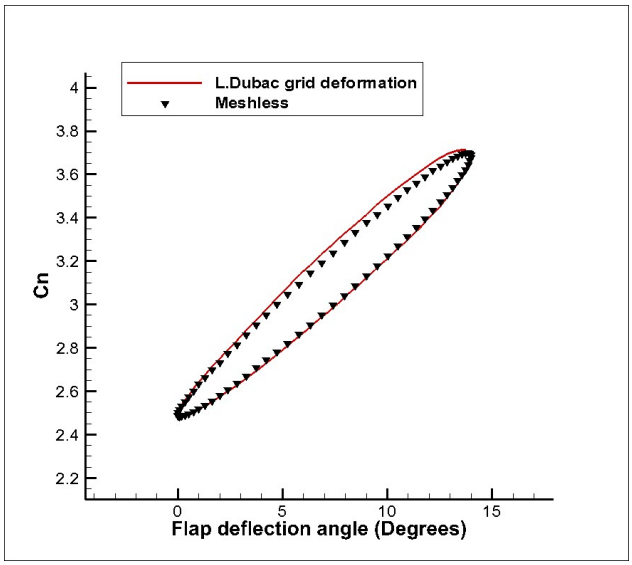

Figure 22 Willams airfoil : lift coefficient variation in flap deflection angle

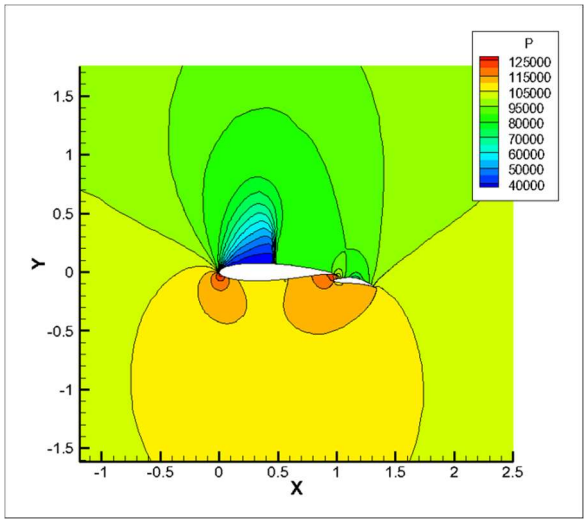

Figure 23 pressure contours for Williams airfoil the oscillating flap (0°)

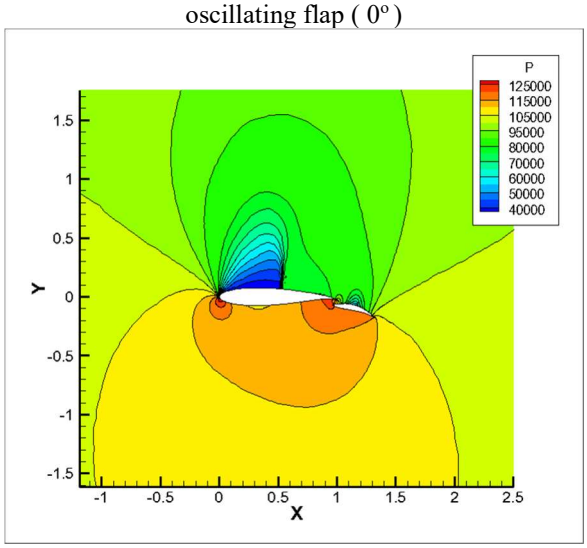

Figure 24 pressure contours for Williams airfoil the oscillating flap (7° pitch down)

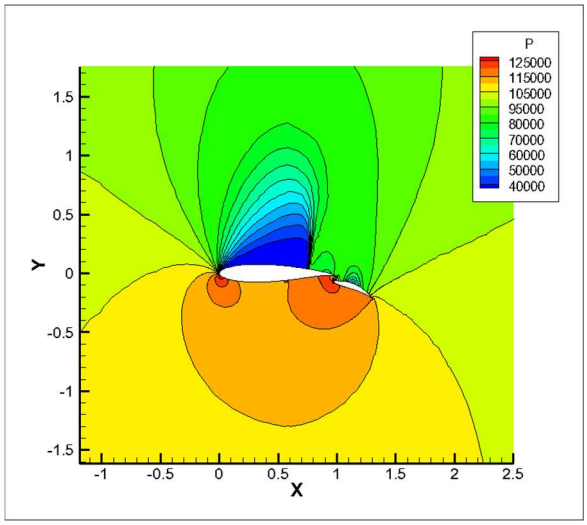

Figure 25 pressure contours for Williams airfoil the oscillating flap (14°)

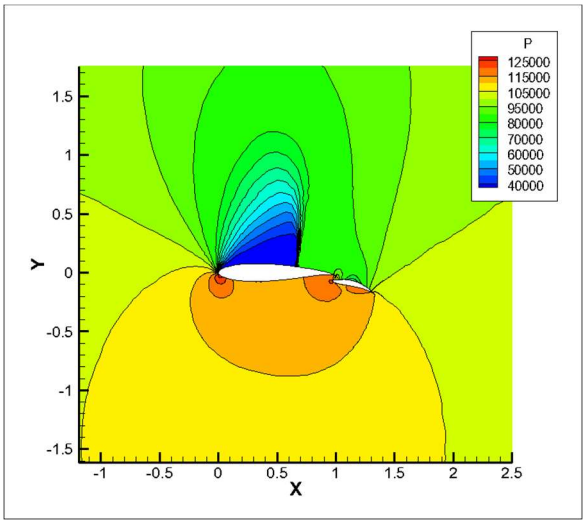

Figure 26 pressure contours for Williams airfoil the oscillating flap (7° pitch up)

5 Conclusion

A point generation technique for the moving systems are suggested. Using the hybrid concept which mixes the prismatic point system and the background point system, an efficient and robust way to solve unsteady problem considering moving multiple boundaries is developed. Three test cases are selected as a validation model. The results suggest that the meshless point generation technique and the meshless flow solver are quite robust, accurate and efficient compared to another methods.

The final goal of a meshless method is to solve highly-complicated and practical problems, such as store separation, shroud separation. In order to achieve the goal, this work will be expanded to three-dimensional case considering multiple objects. Additionally, flight dynamics module or structural analysis module will be contained in this code.

Acknowledgments

- This research was supported by Space Core Technology Program through the National Research Foundation of Korea(NRF) funded by the Ministry of Science, ICT & Future Planning(NRF-2015M1A3A3A05027630)

- This work was supported by the Brain Korea 21 Plus Project in 2016

References

[1] A. Katz, Aaron Jon. Meshless methods for computational fluid dynamics. ProQuest, (2009).

[2] Zhou, Xing, and Houqian Xu. "Gridless method for unsteady flows involving moving discrete points and its applications." Engineering Applications of Computational Fluid Mechanics 4.2 (2010): 276-286.

[3] Ortega, Enrique, et al. "A meshless finite point method for three-dimensional analysis of compressible flow problems involving moving boundaries and adaptivity." International Journal for Numerical Methods in Fluids 73.4 (2013): 323-343.

[4] Huh, Jin Young, Kyu Hong Kim, and Suk Young Jung. "Meshless Method for Simulation of Compressible Reacting Flow.", “International Council of the Aeronautical Sciences”, Saint Petersburg, Russia (2014).

[5] Steve Karman Jr, L. "SPLITFLOW-A 3D unstructured Cartesian/prismatic grid CFD code for complex geometries." (1995).P. Lancaster and K. Salkauskas. Surfaces generated by moving least squares methods. Math. Comput. 37: 141–158, 1981.

[6] Landon R, “NACA 0012 oscillating and transient pitching compendium of Unsteady Aerodynamic Measurements, Data Set. AGARD Report R-702”, August 1982

[7] Williams, B. R. An exact test case for the plane potential flow about two adjacent lifting aerofoils. HM Stationery Office, 1971.

[8] Kim, Kyu Hong, Chongam Kim, and Oh-Hyun Rho. "Methods for the accurate computations of hypersonic flows: I. AUSMPW+ scheme." Journal of Computational Physics 174.1 (2001): 38-80.

[9] S. Yoon and A. Jameson. Lower-Upper Symmetric-Gauss-Seidel Method for the Euler and Navier-Stokes Equations, AIAA Journal, 26(9): 1025-1026, 1988.

[10] Dubuc, L., et al. "A grid deformation technique for unsteady flow computations."International journal for numerical methods in fluids 32.3 (2000).

[11] Chen H Q and Shu C. “An Efficient Implicit Mesh-Free Method TO solve Two-Dimensional Compressible Euler Equations”, international *Journal of Modern Physics* C., Vol. 16, No. 3, pp 439-454, 2005.

[12] Rhee, Jae-Sang, et al. "Three dimensional meshless point generation technique for complex geometry.", The 2015 World Congress on Aeronotics, Nano, Bio, Robotics, and Energy (ANBRE15), Incheon, Korea, August 2015.

[13] Kirshmen, D. J., and F. Liu. "Flutter prediction by an Euler method on non-moving Cartesian grids with gridless boundary conditions." Computers & fluids35.6 (2006): 571-586.

[14] Mavriplis D J. Revisiting the least-squares procedure for gradient reconstruction on unstructured meshes, AIAA paper 2003-3986, AIAA 16th Computational Fluid Dynamics Conference, 2003.

Contact Author Email Address

Mailto:aerocfd1@snu.ac.kr

Copyright Statement